Hydrological Research Letters **15**(2), 37–43 (2021)
Published online in J-STAGE (www.jstage.jst.go.jp/browse/hrl). DOI: 10.3178/hrl.15.37

Detectability of variation in river flood from satellite images

Yukiko Hirabayashi[1], Haireti Alifu[1], Dai Yamazaki[2], Gennadii Donchyts[3] and Yuki Kimura[4]
[1]*Department of Civil Engineering, Shibaura Institute of Technology, Japan*
[2]*Institute of Industrial Science, The University of Tokyo, Japan*
[3]*Faculty of Civil Engineering and Geosciences, Delft University of Technology, the Netherlands*
[4]*Corporate Planning Department, MS&AD InterRisk Research & Consulting, Inc., Japan*

Abstract:

Floods are major natural disasters that have considerable consequences worldwide. As the frequency and magnitude of flooding are expected to be affected by ongoing climate change, understanding their past changes is important for developing adequate adaptation measures. However, the limited spatiotemporal coverage of flood gauges hinders detection of changes in flooding, particularly in poorly gauged regions. Here, we propose a method using surface water data of river floodplain inundation as a proxy of the magnitude and frequency of flooding. Surface water data − Aqua Monitor which represented the probability linear trend changes in land and water surface area based on 30-m Landsat images between 1984–2000 and 2000–2013 was used in this study. The changes in water surface area over the floodplain obtained from Aqua Monitor showed high correspondence with historical trends observed or simulated annual maximum daily discharge, indicating the potential to detect changes in frequency and magnitude of flood from satellite data. In regions where changes could be measured with sufficient satellite images, 29% showed an increase in water surface area in the flood plain, 41% showed a decrease, and 30% showed small or no changes.

KEYWORDS flood; flood plain; satellite-based inundation area; CaMa-Flood

INTRODUCTION

Flooding is a common major natural hazard in many areas of the world, and directly affects people's lives and livelihoods. Global warming will increase the frequency of floods, especially in Asia and Africa where rapid growth of the population and assets are expected (Hirabayashi *et al.*, 2013). However, changes in flooding in these regions are poorly understood due to limited numbers of *in situ* observations.

A satellite remote sensing-based approach has been widely applied for assessing recent changes in water surface area, including flood changes. For example, Najibi and Devineni (2018) showed an increase in the frequency and duration of floods worldwide using a global flood database based on water surface area images derived from remote sensing satellites. Ji *et al.* (2018) generated the 500-m Resolution Daily Global Surface Water Change Database (DGSWCD500m), derived from more than 1.9 million frames of the MODIS surface reflectance product (MOD09GA) from 2001 to 2016 which have high potential applicability to the determination of flood inundation. Donchyts *et al.* (2016) developed a Deltares Aqua Monitor, which shows a global map of water and land surface area changes over 1984–2013 at 30 m spatial resolution using the multi-petabyte archive of millions of Landsat series images. It contained probability linear trend changes in land and water surface area, and this information around river floodplain reflects the river flood dynamic. Hence, assessing the utility of high-resolution water surface data for revealing changes in river flooding patterns is possible and important, especially in data-poor regions.

The aims of this study are to: (1) evaluate the ability of the satellite-based water surface area change in a floodplain to detect changes in magnitude and frequency of flood during 1984–2013 by comparing those of *in situ* observations or simulated river discharge, and (2) discuss the observed changes in satellite-derived water surface area and peak discharge data at global scale.

DATA AND METHODS

The high-resolution Multi-Error-Removed Improved Terrain (MERIT) global digital elevation model (DEM) (Yamazaki *et al.*, 2019), stream gauge station data from the Global Runoff Data Center (GRDC), global daily discharge reanalysis, and Aqua Monitor (Donchyts *et al.*, 2016), are the main data used for this study. Other auxiliary data, such as the FLOod PROtection Standards, FLOPROS (Scussolini *et al.*, 2016), dam index derived from GRanD (Lehner *et al.*, 2011), percent tree cover data (Kobayashi *et al.*, 2016), DGSWCD500m (Ji *et al.*, 2018), and Emergency Events Database, EM-DAT (Guha-Sapr *et al.*, 2016) are also used for this study. Detailed information for data used in this study is available in the supplementary materials (SM) (Table SI–SIII).

In order to detect the flood variation, it is necessary to perform several preprocessing steps, such as upscaling, masking out pixels that are out of the river floodplain, measuring pixel changes in the sub-basins scale and manmade

Correspondence to: Haireti Alifu, Department of Civil Engineering, Shibaura Institute of Technology, 3-7-5 Toyosu, Koto-ku, Tokyo 135-8548, Japan. E-mail: haireti.alifu.f4@sic.shibaura-it.ac.jp

Received 5 April, 2021
Accepted 18 May, 2021
Published online 22 June, 2021

large surface area changes, and excluding locations where there were too few satellite observations. Detailed descriptions of the datasets and the method are provided in the following sections.

Global floodplain and sub-catchment data

To remove water pixels outside of the floodplain, 1 min resolution of a global floodplain area was generated from the MERIT DEM (Yamazaki *et al.*, 2019). The MERIT DEM was generated through removal of multiple errors from existing DEMs, and performs better than similar previous products. The floodplain was defined as the area within 5 km of major rivers (total drainage area >3,000 km^2) with a water surface height of <10 m. The MERIT DEM was also used to define 445 global sub-catchments with areas >100,000 km^2. The inundation area of each sub-catchment was then analyzed.

Stream gauge data and global daily discharge reanalysis

Data for 70 stream gauge stations were provided by the GRDC (https://www.bafg.de/GRDC/EN/Home/homepage_node.html). These stations are selected based on the following criteria: 1) stations have larger drainage basin area (area >100,000 km^2) and long-term discharge data (at least 30 years of observed daily discharge data for the period 1975–2015 and data were missing for fewer than 73 days in the year, i.e. 20% of the year), 2) stations are located at or near the outlet region of the sub-catchment. Moreover, if there were several GRDC stations in the same sub-catchment, we analyzed the data from the station with the largest drainage basin (Figure S1).

On the other hand, discharge reanalysis for the 1984–2013 period was performed using a river and inundation model, the CaMa-Flood, using daily runoff input derived from a land surface model driven by bias-corrected meteorological reanalysis (Tanoue *et al.*, 2020, Text S1). CaMa-Flood realistically simulates floodplain inundation dynamics and improves predictions of daily scale river discharge, at the high spatiotemporal resolution, by incorporating floodplain inundation dynamics (Yamazaki *et al.*, 2011). Evaluation of discharge reanalysis indicated that (Figure S1–S2) peak discharge has a good correlation with most of the peak discharge derived from GRDC. However, lower correlation coefficients (R) were estimated in the cold river catchment and highly regulated river catchment due to the CaMa-Flood model does not consider human river management activities of reservoirs, irrigation, or land use. Hence, the modeled discharge reflects flood changes driven by natural hydrological processes (e.g. changes in precipitation, snow, and evapotranspiration). Despite the inevitable biases, as the discharge reanalysis showed anomalous high peaks in flood years, we assume that the discharge reanalysis can be used as a proxy of the magnitude of the flood where *in situ* observation was unavailable.

Satellite-derived water surface area changes between 1984–2013

Aqua Monitor (Donchyts *et al.*, 2016), performed water-land and land-water surface area change by calculating linear regression of the wetness index values derived from a large number of Landsat series images at 30 m pixel. The proportions of pixels showing an increase (land to water) or decrease (water to land) over the floodplain of each sub-catchment was calculated based on existence of water pixels between the period of 1984–2000 and 2000–2013. As Landsat has a 16-day interval, it has sufficient opportunity to detect inundation area extent due to flooding in large river basins having large river extent for a month or more (Bender, 1991). We assume that the increase or decrease of water pixels within inundation area reflects changes in frequency or magnitude of flooding between the two periods.

To minimize the effects of artificial and natural river changes, such as shifting, capturing, and straightening of river channels, we first scaled the original images (30 m) up to a resolution of 1 min (~1.84 km) and then measured the increase or decrease in the number of water pixels in the river floodplain using floodplain and sub-basin masks defined by the MERIT DEM. We expected the upscaling procedure to cancel-out the increase and decrease of water pixels associated with route management and natural river shifting. The average linear trend change values in land and water surface area were then calculated over the floodplain in each sub-catchment. To exclude locations where there were too few satellite observations to determine the change in inundation extent, we selected sub-catchments with on average >170 Landsat images between 1984 and 2013. To avoid images of small inundation areas, the proportion of water pixels in the analyzed floodplains of each sub-catchment was required to be >15%. Eighteen sub-catchments with new reservoir construction after 2000 were removed from the analysis using reservoir and dam data of GRanD because the number of water pixels was considered to have increased due to new reservoir construction (Text S2, Figure S3). Finally, we selected and analyzed 177 sub-catchments.

Generally, heavy rainfall induced floods cause an immediate response (lasting from only a few hours to a few days) in small streams, but in large rivers, flood runoff may exceed channel capacity for more than a month (Bender, 1991). Ponds are a very common and abundant habitat in natural floodplains. Large extreme flooding always created ponds/lakes or expanded the area of ponds/lakes that already exist in the natural floodplain. These ponds/lakes can keep their area for a long time (except in arid regions) as they are regularly flooded or are connected to a river. Thus, land-water and water-land change information from Aqua Monitor has the potential to represent flood trend in the case of a large river basin. Our analysis of DGSWCD500m (Text S3), which has a lower spatial resolution than the Landsat images implemented in Aqua Monitor, using a method similar to that of Alifu *et al.* (2019), confirmed the ability of satellite-derived daily water surface area data to detect the instantaneous magnitude of flood events, when and where large floods occurred in the past, especially when the magnitude of the past flooding was large (return period >100 years) (Figure S4–S6 and Table SII). Importantly, it also supports the view that satellite-derived water surface area can detect flood events in regions with high flood protection (Text S3).

Trends in the annual maximum daily discharge

The trends in flooding were analyzed for 177 global sub-catchments using gauge data (Figure S7a), the daily dis-

charge reanalysis (Figure S7b), and Aqua Monitor (Figure S7c). The percentage changes per year in the observed annual maximum daily discharge (GRDC) were calculated by fitting values to a linear trend in the latest 30 years between 1975 and 2015, with the available observed period varying for each station. The same calculation was performed for discharge reanalysis using data from 1984–2013.

For the global analysis of trends in flooding, the discharge analysis at the outlet pixel which has the largest accumulated flow within the sub-catchment, defined by a river routing network in CaMa-Flood, was calculated to represent the discharge in that sub-catchment.

RESULTS AND DISCUSSION

Evaluation of flood change

To determine whether the satellite-derived surface area change reflected historical trends in river flooding, the data were compared with the observed annual maximum daily discharge data for 22 sub-catchments where tributaries had little effect (Table I and Figure S8). By tracking changes in the proportion of water pixels using Aqua Monitor, we were able to detect cases showing the same direction of change in observed annual maximum daily discharge. Of 22 basins, 19 showed the same direction of change. Among these, 12 showed increased flooding, and 7 showed a decrease.

However, in three basins (Missouri, Burdekin, and Snake), although the observed annual maximum daily discharge showed increasing trends, the inundation areas, as analyzed using Aqua Monitor, exhibited decreasing trends. One potential reason for the discrepancy is the effect of the water surface area of reservoirs. Because we defined floodplains according to the distance from the main river, water pixel changes may reflect changes in water surface area due to reservoirs located along the main channel of the river. To know the effects of reservoir/dam to river discharge, we calculated the dam index (Figure S3) as the total volume of reservoirs in the upper basin obtained from the Global Reservoir and Dam Database (GRanD) (Lehner *et al.*, 2011) divided by the average daily discharge for the period 1958–2013. Table I and Figure S3 indicated the Missouri River is highly controlled, as shown by the high dam index. There were several flood events during the analysis period, which caused increasing trends in both the observed and discharge reanalysis annual maximum discharge. However, at the same time, the Missouri river basin experienced a prolonged drought between 2000 and 2007, which caused a significant decrease in reservoir storage (Gao *et al.*, 2012) that could have been responsible for the decreasing trend in

Table I. Summary of past changes in flood in 22 selected basins for which observations are available from the Global Runoff Data Centre (GRDC). Numbers in the table correspond to the location map in Figure S8a. *, $p < 0.10$; ** $p < 0.05$

	River name	GRDC ID	Observation (% yr^{-1})	Aqua Monitor (10^{-3} % yr^{-1})	Discharge reanalysis (% yr^{-1})	Dam index 1975–2011	Protection level
1	Yukon	4103800	0.14	0.25	–0.40	0	47
2	Peace	4208450	–0.06	–0.11	0.76	0	47
3	North	4213440	0.42	0.05	0.11	0	47
4	South	4213400	3.76*	0.07	0.34	8.86	48
5	Assiniboine	4213650	2.40*	0.46	0.90	0.75	51
6	Ohio	4123050	0.13	0.10	–0.07	2.14	149
7	Mississippi	4119300	1.34*	0.02	0.34	3.37	78
8	Yellowstone	4120950	1.08	0.03	–0.35	2.18	51
9	Missouri	4120900	1.93	–0.26	0.95	22.64	52
10	Red	4126801	–2.10	–0.05	–0.30	10.46	139
11	Colorado	4150450	–1.15	–0.92	0.69	7.37	67
12	Colorado	4152103	–0.75	–1.30	0.18	38.77	123
13	Snake	4116181	1.12	–0.13	0.43	8.35	76
14	Rio Jurua	3624120	0.04	0.10	0.69	0	18
15	Rio Purus	3625340	0.14**	0.09	0.77*	0	18
16	Sao	3651807	–2.10**	–1.97	–0.85	62.18	39
17	Severnaya	6970250	–0.40	–0.05	0.67	0	49
18	Don	6978250	–2.22*	–0.46	–0.20	21.10	51
19	Fitzroy	5101301	1.33	0.13	0.60	1.35	49
20	Burdekin	5101200	3.40	–0.11	2.38	1.64	49
21	Okavango	1257101	1.62	0.06	0.38	0	17
22	Kwando	1291200	2.07	1.15	7.45**	0	17

water surface area detected by Aqua Monitor. Similarly, the Burdekin river basin experienced a severe drought between 2005 and 2006 that caused a reduction in the amount of water stored in the Burdekin Falls Dam. This drought might have been the main cause of the decreasing trend in the inundation area calculated using Aqua Monitor. Additionally, several floods occurred in the Burdekin River between 2000 and 2013. These floods may have caused the increasing trends in the observed and discharge reanalysis annual maximum daily discharge.

Another potential reason for these trends is water management; for example, there are five streamflow gauges in the same sub-catchment of the Snake River, and our analysis showed an increasing trend (+ 1.12% yr^{-1}) based on the observation data of the station situated within the largest drainage basin area, whereas the remaining four gauges at upstream locations showed decreasing trends (ranging from –0.20 to –2.26% yr^{-1}). This may have been due to intensive irrigation activities. The increasing trend of the gauge located farthest downstream was less affected by the irrigation activities due to return flows from surface water irrigation (Hoekema and Sridhar, 2011). The satellite-derived trend in the water surface area showed similar direction of trend change with the observed trend (Table I and Figure S8) and indicated that exclusion of reservoirs from the floodplain mask and consideration of irrigation water usage would increase the likelihood of detecting changes in flooding trends.

Comparison of discharge reanalysis with observed discharge and satellite-derived water surface area changes indicated that human water management activities may have had an effect. In the Yukon, Peace, Ohio, Yellowstone, Colorado, and Severnaya river basins, the annual maximum daily discharge of discharge reanalysis showed the opposite trend to those of observed discharge and satellite-derived water surface changes. Several sub-catchments showed increasing trends in discharge reanalysis but decreasing trends in observed or satellite-based inundation area. For example, the discharge reanalysis showed increases in flooding in two Colorado basins, and in the Peace and Severnaya River basins, whereas observed and satellite-derived flood areas showed decreasing trends. Conversely, discharge reanalysis indicated that the likelihood of flooding decreased in the Ohio, Yukon, and Yellowstone River basins, but observed discharge and satellite-derived data indicated that the occurrence of flooding increased.

The discrepancies between the discharge reanalysis and observed trends suggested that human activities leading to a reduction in peak floodwater and reservoir operations affected river discharge, as the model did not consider river management activities. We assumed that when the dam index was larger, river discharge was more affected by reservoir operations in the upstream area. The results showed substantial reservoirs along the Ohio, Yellowstone, and Colorado Rivers (Table I), indicating that reservoir operations or other river management activities affect flood trends. Other potential sources of discrepancy include uncertainties in modeled hydrological processes and climate inputs. The current modeling framework cannot replicate ice jam flooding, which is the main cause of floods in the Peace, Yukon, and Severnaya basins (Beltaos, 2018; Brabets *et al.*, 2000; Peters and Prowse, 2001; Vuglinsky, 2002). Although discharge reanalysis has been used as a good indicator to show changes in river flooding where *in situ* observation is unavailable (e.g. Alfieri *et al.*, 2020), additional information derived from satellite images compensate for its disadvantage in particular for basins with human water management.

We also evaluated the effects of local flood protection measures on the ability to capture flooding trends using the global database of FLOPROS (Scussolini *et al.*, 2016, Text S4, Table I and Figure S9). The result in Table I shows that the flooding trend derived using Aqua Monitor is in the same direction as the actual trend, although these catchments vary in flood protection level. This illustrated that despite levees and other flood-protection measures, Aqua Monitor can detect high volumes of water, changes in river width between levees, and changes in natural inundation area (including flood retention ponds).

Despite the discrepancy between the modeled and actual results for some basins, due mainly to the effects of human activities, 19 of 22 events for which observation data were available showed concordance in the direction of change between the satellite- and gauge observation-derived trends. Thus, satellite-based water surface area changes in a floodplain have a potential to detect changes of extension of flood water (particularly important in poorly gauged regions) within the observed time in Aqua Monitor, which may relate to both frequency and magnitude of flooding. This illustrated that despite levees and other flood-protection measures, or some potential impacts of land use change along rivers, Aqua Monitor can detect high volumes of water, changes in river width between levees, and changes in natural inundation area (including flood retention ponds).

Water surface area change analysis at the global scale

In regions where changes could be measured with sufficient satellite images from Aqua Monitor, 29% showed an increase in water surface area in the flood plain, 41% showed a decrease, and 30% showed small or no changes. Additional trend data from Aqua Monitor provided a wider view of past water surface area changes in data-poor regions (Figure 1b). For example, increasing trends were found across the upper Amazon, and in several basins in East Asia. There were decreasing trends in southeastern Australia, eastern Brazil, Argentina, and the western part of Southeast Asia. These results are consistent with a study based on observed peak discharges in the period 1971–2010 (Gudmundsson *et al.*, 2019). Our results showed similar upward and downward trends in the United States (Archfield *et al.*, 2016) and Western Europe (Blöschl *et al.*, 2019).

Considering the relatively high concordance between the observed annual maximum daily discharge and satellite-derived flood area change, the results increase our understanding of trends in water surface area, which may shed light on past flooding events, especially in South America and Southeast Asia where *in situ* observations are limited. We expect that the continuing accumulation of satellite images will enhance our understanding of trends in flooding over a larger area in the future.

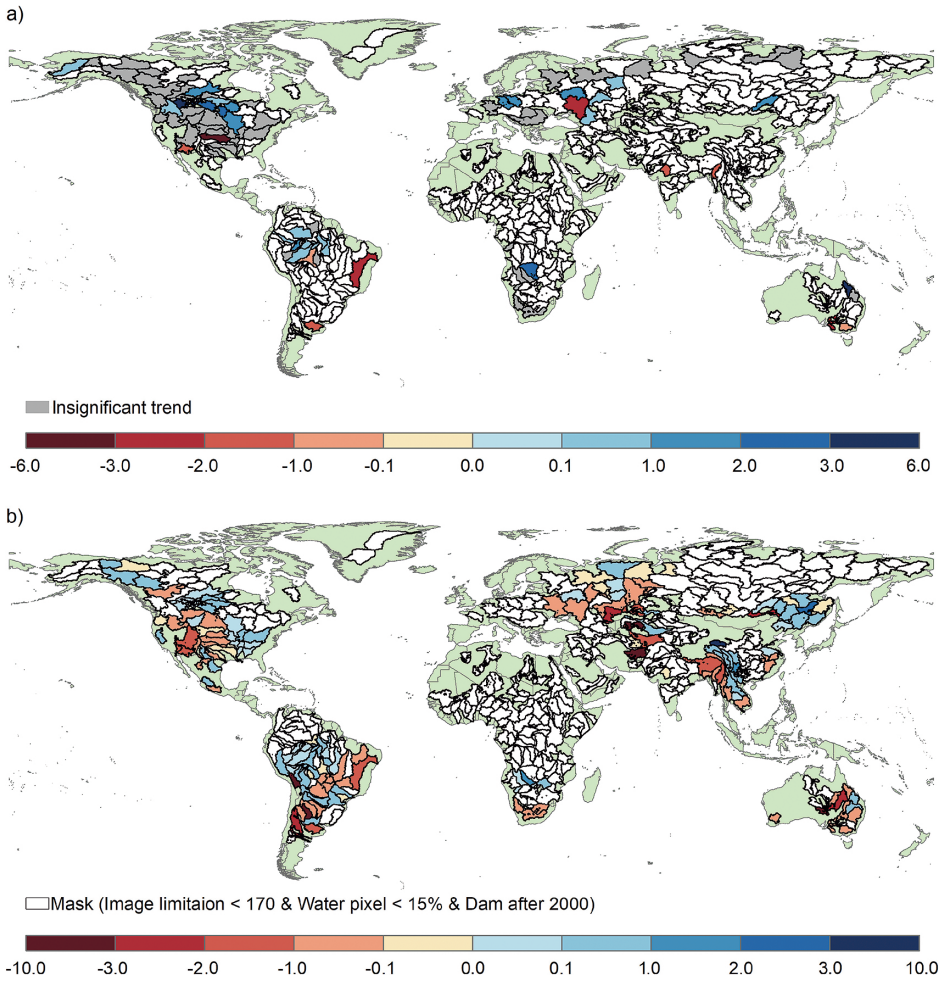

Figure 1. Detected trends in historical floods over the past few decades. a) Trends in the observed and simulated annual maximum daily discharge (% yr^{-1}). Trends were plotted only when they were in the same direction as that seen in the satellite-derived inundation area data. b) Trends in inundation area derived from satellite data. Sub-catchments (gray and white colored) without significant trends ($p < 0.05$), few satellite images (i.e. <170 for both 1984–2000 or 2000–2013), or a small proportion of water pixels in the inundation area (< 15%) were excluded

CONCLUSIONS

We investigated the utility of a satellite-derived water surface area dataset for detecting past floods on a global scale. The analysis demonstrated the ability of these data to provide information on flood area changes in data-poor basins, such as those in Asia and South America. The surface water area change derived from Aqua Monitor successfully detects direction of changes in flood in most analyzed basins. In addition to the discharge reanalysis, our results showed that satellite-derived surface water change can be utilized to detect occurrence of flooding or past changes in frequency or magnitude of flooding where *in situ* observation is unavailable. In regions where changes could be measured with sufficient satellite images, Aqua Monitor indicated that 29% of the basins experienced an increase in water surface area in the flood plain, 41% experienced a decrease, and 30% experienced small or no change (Figure 1).

Furthermore, comparison of the discharge reanalysis and observed discharge indicated that water management activities potentially affect flooding, particularly in highly regulated river basins. This is indeed the disadvantage of discharge reanalysis which has been often used to analyze river water change at global scale. As the observations and satellite-derived water surface area change showed relatively high concordance in many basins, additional information derived from satellite images would enhance our understanding of flood change where *in situ* observation is unavailable. Moreover, flood trend data obtained from different sources, as well as models incorporating the effects of water management activities, could clarify the mechanism underlying changes in flood trends.

ACKNOWLEDGMENTS

The flooding trend data for the sub-catchments used to draw the figures are available for research purposes upon request. This research was supported by the Environment Research and Technology Development Fund

(JPMEERF20202005) of the Environmental Restoration and Conservation Agency of Japan, a JSPS Grant-in-Aid for Scientific Research (18H01540), the Integrated Research Program for Advancing Climate Models (TOUGOU) (JPMXD0717935457) from the Ministry of Education, Culture, Sports, Science and Technology (MEXT), Japan, and MS&AD InterRisk Research & Consulting, Inc.

SUPPLEMENTS

Text S1. Global daily discharge reanalysis
Text S2. Dam index derived from Global Reservoir and Dam Database (GRanD)
Text S3. Ability of the satellite-derived water surface area to detect historical floods
Text S4. Catchment based global database of FLOod PROtection Standards (FLOPROS)
Figure S1. Correlation of annual maximum daily discharge (1980–2013) derived from GRDC and discharge reanalysis at the 70 GRDC stations located at outlet region of catchment
Figure S2. Scatter plot of annual maximum daily discharge (1980–2013) derived from GRDC ($m^3\ s^{-1}$) and discharge reanalysis ($m^3\ s^{-1}$) based on the 136 GRDC stations
Figure S3. a) Dam index and b) total storage capacity of dam/reservoirs constructed after 2000
Figure S4. Global percentage tree-cover of each catchment
Figure S5. Scatterplot of the median normalized inundation anomaly (($Ey - M$)/SD × 100) for selected flood events (see Table SII) and their return periods. Ey is the total inundation pixels of each sub-basin (ATCIE) from the extreme flood of the year, SD and M is the standard deviation and mean of the ATCIE for the whole period
Figure S6. Location of GRDC stations in the sub-catchments. Cyan lines are the sub-catchment boundaries and red dots are GRDC stations
Figure S7. Changes in the a) observed (units: % yr^{-1}) and b) discharge reanalysis (middle panel) discharges (units: % yr^{-1}), and c) water surface area (units: 10^{-3} % yr^{-1}), as derived from satellite data
Figure S8. Changes in the a) observed (units: % yr^{-1}) and b) discharge reanalysis (units: % yr^{-1}), and c) in water surface area derived from satellite data (units: 10^{-3} % yr^{-1}) for 22 basins
Figure S9. FLOPROS flood protection standards (Scussolini *et al.*, 2016). The average return period (years) of the sub-catchment is shown
Table SI. List of GRDC stations used for validation of discharge reanalysis
Table SII. Summary of selected flood events between 2001 and 2013
Table SIII. Data used in this study

REFERENCES

Alfieri L, Lorini V, Hirpa FA, Harrigan S, Zsoter E, Prudhomme C, Salamon P. 2020. A global streamflow reanalysis for 1980–2018. *Journal of Hydrology X* **6**: 100049. DOI: 10.1016/j.hydroa.2019.100049.

Archfield SA, Hirsch RM, Viglione A, Blöschl G. 2016. Fragmented patterns of flood change across the United States. *Geophysical Research Letters* **43**: 10232–10239. DOI: 10.1002/2016GL070590.

Alifu H, Yamazaki D, Luyan J, Hirabayashi Y. 2019. Investigating flood detectability using satellite-derived daily global surface water change and a high resolution floodplain mask. *Journal of Japan Society of Civil Engineers, Ser. B1 (Hydraulic Engineering)* **75**: 163–168. DOI: 10.2208/jscejhe.75.2_I_163.

Beltaos S. 2018. Frequency of ice-jam flooding of Peace-Athabasca Delta. *Canadian Journal of Civil Engineering* **45**: 71–75. DOI: 10.1139/cjce-2017-0434.

Bender S. 1991. Primer on natural hazard management in integrated regional development planning: *Chapter 8 − Floodplain definition and flood hazard assessment*. Organization of American States, Department of Regional Development and Environment. Executive Secretariat for Economic and Social Affairs, Washington, DC.

Blöschl G, Hall J, Viglione A, Perdigão RA, Parajka J, Merz B, Lun D, Arheimer B, Aronica GT, Bilibashi A, Boháč M, Bonacci O, Borga M, Čanjevac I, Castellarin A, Chirico GB, Claps P, Frolova N, Ganora D, Gorbachova L, Gül A, Hannaford J, Harrigan S, Kireeva M, Kiss A, Kjeldsen TR, Kohnová S, Koskela JJ, Ledvinka O, Macdonald N, Mavrova-Guirguinova M, Mediero L, Merz R, Molnar P, Montanari A, Murphy C, Osuch M, Ovcharuk V, Radevski I, Salinas JL, Sauquet E, Šraj M, Szolgay J, Volpi E, Wilson D, Zaimi K, Živković N. 2019. Changing climate both increases and decreases European river floods. *Nature* **573**: 108–111. DOI: 10.1038/s41586-019-1495-6.

Brabets TP, Wang B, Meade RH. 2000. Environmental and hydrologic overview of the Yukon River Basin, Alaska and Canada. *Water-Resources Investigations Report* 99-4204.

Donchyts G, Baart F, Winsemius H, Gorelick N, Kwadijk J, van de Giesen N. 2016. Earth's surface water change over the past 30 years. *Nature Climate Change* **6**: 810–813. DOI: 10.1038/nclimate3111.

Gao H, Birkett C, Lettenmaier DP. 2012. Global monitoring of large reservoir storage from satellite remote sensing. *Water Resources Research* **48**. DOI: 10.1029/2012WR012063.

Gudmundsson L, Leonard M, Do HX, Westra S, Seneviratne SI. 2019. Observed trends in global indicators of mean and extreme streamflow. *Geophysical Research Letters* **46**: 756–766. DOI: 10.1029/2018GL079725.

Guha-Sapir D, Below R, Hoyois P. 2016. EM-DAT: the CRED/OFDA international disaster database.

Hirabayashi Y, Mahendran R, Koirala S, Konoshima L, Yamazaki D, Watanabe S, Kim H, Kanae S. 2013. Global flood risk under climate change. *Nature Climate Change* **3**: 816–821. DOI: 10.1038/NCLIMATE1911.

Hoekema DJ, Sridhar V. 2011. Relating climatic attributes and water resources allocation: A study using surface water supply and soil moisture indices in the Snake River basin, Idaho. *Water Resources Research* **47**. DOI: 10.1029/2010WR009697.

Ji L, Gong P, Wang J, Shi J, Zhu Z. 2018. Construction of the 500-m resolution daily global surface water change database (2001–2016). *Water Resources Research* **54**: 10270–10292. DOI: 10.1029/2018WR023060.

Kobayashi T, Tsend-Ayush J, Tateishi R. 2016. A new global tree-cover percentage map using MODIS data. *International*

Journal of Remote Sensing **37**: 969–992. DOI: 10.1080/01431161.2016.1142684.

Lehner B, Liermann CR, Revenga C, Vörösmarty C, Fekete B, Crouzet P, Döll P, Endejan M, Frenken K, Magome J, Nilsson C, Robertson JC, Rödel R, Sindorf N, Wisser D. 2011. High-resolution mapping of the world's reservoirs and dams for sustainable river-flow management. *Frontiers in Ecology and the Environment* **9**: 494–502. DOI: 10.1890/100125.

Najibi N, Devineni N. 2018. Recent trends in the frequency and duration of global floods. *Earth System Dynamics* **9**: 757–783. DOI: 10.5194/esd-9-757-2018.

Peters DL, Prowse TD. 2001. Regulation effects on the lower Peace River, Canada. *Hydrological Processes* **15**: 3181–3194. DOI: 10.1002/hyp.321.

Scussolini P, Aerts JCJH, Jongman B, Bouwer LM, Winsemius HC, de Moel H, Ward PJ. 2016. FLOPROS: an evolving global database of flood protection standards. *Natural Hazards & Earth System Sciences* **16**: 1049–1061. DOI: 10.5194/nhess-16-1049-2016.

Tanoue M, Taguchi R, Nakata S, Watanabe S, Fujimori S, Hirabayashi Y. 2020. Estimation of direct and indirect economic losses caused by a flood with long-lasting inundation: application to the 2011 Thailand flood. *Water Resources Research* **56**: p.e2019WR026092. DOI: 10.1029/2019WR026092.

Vuglinsky VS. 2002. Peculiarities of ice events in Russian Arctic rivers. *Hydrological Processes* **16**: 905–913. DOI: 10.1002/hyp.365.

Yamazaki D, Kanae S, Kim H, Oki T. 2011. A physically based description of floodplain inundation dynamics in a global river routing model. *Water Resources Research* **47**: DOI: 10.1029/2010wr009726.

Yamazaki D, Ikeshima D, Sosa J, Bates PD, Allen GH, Pavelsky TM. 2019. MERIT Hydro: a high-resolution global hydrography map based on latest topography dataset. *Water Resources Research* **55**: 5053–5073. DOI: 10.1029/2019WR024873.